Hybrid-exchange density-functional theory study of the electronic structure of MnV_2O_4: Exotic orbital ordering in the cubic structure

Wei Wu*

Department of Electronic and Electrical Engineering and London Centre for Nanotechnology, University College London, Gower Street, London WC1E 6BT, United Kingdom

(Received 15 February 2015; revised manuscript received 21 April 2015; published 7 May 2015)

The electronic structures of cubic and tetragonal MnV_2O_4 have been studied using hybrid-exchange density-functional theory. The computed electronic structure of the tetragonal phase shows an antiferro-orbital ordering on V sites and a ferrimagnetic ground state (the spins on V and Mn are antialigned). These results are in good agreement with the previous theoretical result obtained from the local-density approximation + U methods [S. Sarkar *et al.*, Phys. Rev. Lett. **102**, 216405 (2009)]. Moreover, the electronic structure, especially the projected density of states of the cubic phase, has been predicted with good agreement with the recent soft x-ray spectroscopy experiment. Similar to the tetragonal phase, the spins on V and Mn in the cubic structure favor a ferrimagnetic configuration. Most interesting is that the computed charge densities of the spin-carrying orbitals on V in the cubic phase show an exotic orbital ordering, i.e., a ferro-orbital ordering along [110] but an antiferro-orbital ordering along $[\bar{1}10]$.

DOI: 10.1103/PhysRevB.91.195108 PACS number(s): 71.15.Mb, 75.47.Lx, 75.50.Gg, 75.25.Dk

I. INTRODUCTION

Many fascinating phenomena in condensed-matter physics were discovered in transition-metal oxides (TMOs) and their closely related compounds, such as the first high-transition-temperature superconductivity in $YBaCuO_3$ [1,2]. An important ordering phenomenon, orbital ordering (OO), has a long history in the physics of TMOs, back to the 1930s, when the concept of charge ordering in Fe_3O_4 was proposed [3]. OO occurs when the orbital degeneracy is lifted essentially by the interaction with the lattice environment [4,5]. The best-known example of OO is the Jahn-Teller (JT) distortion observed in $LaMnO_3$ [6]. Therein the e_g degenerate manifold (d_{z^2} and $d_{x^2-y^2}$) in a cubic environment is further split by the JT distortion owing to partial filling of electrons. The underlying physics in OO has been well accounted for by the so-called Kugel-Khomskii model [7]. Most experimental and theoretical works so far have been focused on the system with partially filled e_g orbitals, i.e., e_g active. This type of orbital occupancy can lead to the strongest JT effect because the related d orbitals directly point to ligands and strongly hybridize with the $2p$ orbitals of the anion.

Recently, much attention has been paid to vanadium spinels AB_2O_4 (A = Mg, Co, Fe, Mn, Cd, etc., and B = V) [8–13] owing to their fascinating spin and orbital orderings accompanied by complex structural transitions at low temperature. The interplay between structure, orbital, and spin implies that the underlying physics could be very interesting and that there might be large application potential for these materials. For example, artificially tuning structure by applying an external magnetic field can be thought of as a prototype of TMO-based metamaterials or even quantum metamaterials [11,14]. Another unique point for vanadium spinels is that they are t_{2g} active, in sharp contrast to most of the known TMOs showing OO. In this type of compound, the V^{3+} ions on the B sites form a pyrochlore lattice. The two d electrons on V occupying two t_{2g} orbitals lead to a total spin of $S = 1$, resulting in a t_{2g}-active OO. The OOs in this type of compound can be further complicated by their intrinsic geometrical frustration. In 1939, the charge ordering on the B-site pyrochlore lattice was proposed to cause a sharp increase of the electrical resistivity when cooling below $\sim$120 K in Fe_3O_4 (the "Verwey" transition) [3]. Anderson was the first to realize the intimate relationship between the proton ordering in ice, the Verwey charge ordering, and the ordering of Ising spins [15]. Regardless of the specific material types, geometrical frustration plays a crucial role in determining the spin or charge configurations by minimizing exchange or Coulomb energies. This will, in turn, trigger many interesting phenomena such as orbital-glass and orbital-ice states [16–18]. In addition, the much faster response of electron charges compared to electron spins will find many potential applications in advanced electronics such as orbitronics [19].

MnV_2O_4 (see Fig. 1), in which the Mn^{2+} ion is in a d^5 half-filled high-spin configuration ($S = \frac{5}{2}$), first experiences a magnetic transition to the collinear ferrimagnetic state at $T = 56$ K and then a structural distortion at a slightly lower temperature $T = 53$ K, along with a transition to the noncollinear ferrimagnetic state [20,21]. The observed magnetic ordering below $T = 56$ K is ferrimagnetic; that is, the magnetic moments on Mn^{2+} and V^{3+} are antialigned. In the structural transition, the symmetry is lowered from cubic to tetragonal. The OO of the ground state in the tetragonal MnV_2O_4 structure has been shown theoretically [12] as an A-type antiferro-orbital ordering with a propagation vector of (002).

Previously, the electronic structure and magnetic properties of tetragonal MnV_2O_4 have been investigated theoretically using the local-density approximation (LDA) + U method [12], where an orbital ordering among V^{3+} was proposed, along with a noncollinear magnetic ordering. Following this first-principles calculation, an analytical modeling [22] has further confirmed that an antiferro-orbital ordering exists in tetragonal MnV_2O_4. On the other hand, the electronic structure (especially OO) and magnetic properties of *cubic* MnV_2O_4

*wei.wu@ucl.ac.uk

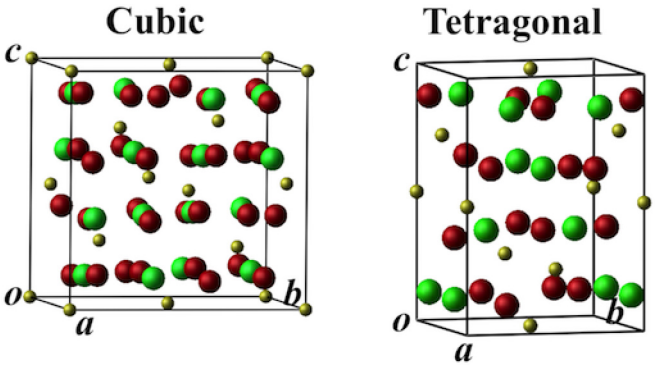

FIG. 1. (Color online) Conventional cells in the (left) cubic and (right) tetragonal MnV_2O_4 crystal structures are shown. Mn is depicted as small yellow balls, V as large green balls, and O as large red balls.

are yet to be studied in detail. It might be worthwhile (i) to employ a computational method without any adjustable parameters, (ii) to take into account the electron correlation properly, and (iii) to compare the electronic structures of cubic and tetragonal MnV_2O_4. Hybrid-exchange density-functional theory (HDFT), in which the exact exchange is hybridized with the generalized gradient approximation (GGA) functional to localize d electrons, has performed well for a wide range of inorganic and organic compounds [23,24]. In this paper, HDFT with the Perdew-Burke-Ernzerhof0 (PBE0) functional [25] has been used to study the electronic structure and magnetic properties of cubic and tetragonal MnV_2O_4. The results presented here not only agree with the previous theoretical and recent experimental studies but also point to an exotic OO state that mixes ferro-orbital and antiferro-orbital orderings. The rest of the discussion is organized as follows: in Sec. II computational details are introduced, in Sec. III the calculation results are presented and discussed, and in Sec. IV some general conclusions are drawn.

II. COMPUTATIONAL DETAILS

The calculations of the electronic structures of tetragonal and cubic MnV_2O_4 were carried out using DFT and hybrid-exchange functional PBE0 as implemented in the CRYSTAL 09 code [26]. The crystal structures of cubic (space group $Fd\bar{3}m$) and tetragonal (space group $I4_1/amd$) MnV_2O_4 experimentally determined in Ref. [11] have been adopted here to perform all the calculations. The basis sets for the atomic orbitals centered on the Mn [27], V [28], and O [29] atoms, which are designed for solid-state compounds, were used. The Monkhorst-Pack samplings [30] of reciprocal space were carried out by choosing a grid of shrinking factor to be $6 \times 6 \times 6$ ($6 \times 6 \times 5$) to be consistent with the ratios among reciprocal lattice parameters for cubic (tetragonal) MnV_2O_4. The truncation of the Coulomb and exchange series in direct space was controlled by setting the Gaussian overlap tolerance criteria to 10^{-6},10^{-6},10^{-6},10^{-6}, and 10^{-12} [26]. The self-consistent field (SCF) procedure was converged to a tolerance of 10^{-6} a.u. per unit cell. To accelerate convergence of the SCF process, all the calculations have been converged using a linear mixing of Fock matrices by 30%.

Electronic exchange and correlation are described using the PBE0 hybrid functional [25], which is free of any empirical or adjustable parameters. The advantages of PBE0 include a partial elimination of the self-interaction error and balancing the tendencies to delocalize and localize wave functions by mixing a quarter of Fock exchange with that from a GGA exchange functional [25]. The broken-symmetry method [31] is used to localize collinear opposite electron spins on atoms in order to describe the antiferromagnetic state.

III. RESULTS AND DISCUSSIONS

A. Projected densities of states

The projected densities of states (PDOSs) of the cubic and tetragonal MnV_2O_4 structures for the antiferromagnetic (AFM) configuration (the spins on Mn and V are antialigned) are shown in Fig. 2. The zero energy is aligned with the valence-band maximum (VBM).

In the cubic and tetragonal structures, the Mn $3d$ PDOS [Figs. 2(a) and 2(b)] shows that the five d orbitals, including $d_{x^2-y^2}$, d_{z^2}, d_{xz}, d_{yz}, and d_{xy}, are singly occupied, thus giving a spin-$\frac{5}{2}$. From the analysis of Mulliken spin densities and the V $3d$ PDOS [Figs. 2(c) and 2(d)], the two electrons occupying t_{2g} states can be identified as the origin of the OO in both cubic and tetragonal MnV_2O_4. In the cubic phase, the molecular orbitals delocalized among the three t_{2g} states are occupied, whereas in the tetragonal phase, only d_{xz} and d_{yz} are involved. The O $2p$ PDOSs [Fig. 2(e)] for the cubic phase are much more delocalized than those for the tetragonal phase [Fig. 2(f)]; this might be due to the elongation of the lattice vectors a and b in the tetragonal structure. The O $2p$ PDOSs are particularly dominant at $\sim$5 eV below the VBM for both the cubic and tetragonal structures, which overlap with the rather weak Mn $3d$ and V $3d$ PDOSs. The O $2p$ orbitals involved here will give rise to the so-called oxygen bonding states that feature the hybridization between the d orbitals on transition metals and p orbitals on O atoms. In addition, it can be observed by comparing the spin-up and spin-down PDOSs that the O $2p$ states have been strongly spin polarized by the magnetic moments on Mn and V. The PDOSs onto the V sites have also been compared with the previous results obtained by the LDA + U [12], which suggests that there is qualitative agreement between them except that the DFT band gap computed here ($\sim$3 eV) is larger than the previously computed one ($\sim$1.1 eV) [12] and the observed one ($\sim$1.1 eV) [32]. The computed O $2p$ PDOSs are in good agreement with the intensities measured in the recent K-edge x-ray absorption and emission spectra; the combination of the theoretical work and experiments will be published in a forthcoming paper [33].

The computed crystal-field splittings between t_{2g} and e_g states ($10Dq$) of Mn^{2+} and V^{3+} in cubic MnV_2O_4 can be read from the energy difference between the two peaks for the t_{2g} and e_g manifolds (shown by the blue arrows) in Figs. 2(a) and 2(c), which are $\sim$1 and $\sim$1.2 eV, respectively. On the other hand, in tetragonal MnV_2O_4, for both Mn^{2+} and V^{3+}, $d_{x^2-y^2}$ and d_{xy} are closely aligned, while the other three $3d$ orbitals overlap well, as shown in Fig. 2(b). This picture is consistent with the previous calculations reported in Ref. [12]. The crystal-field splitting between these two groups is $\sim$1 eV.

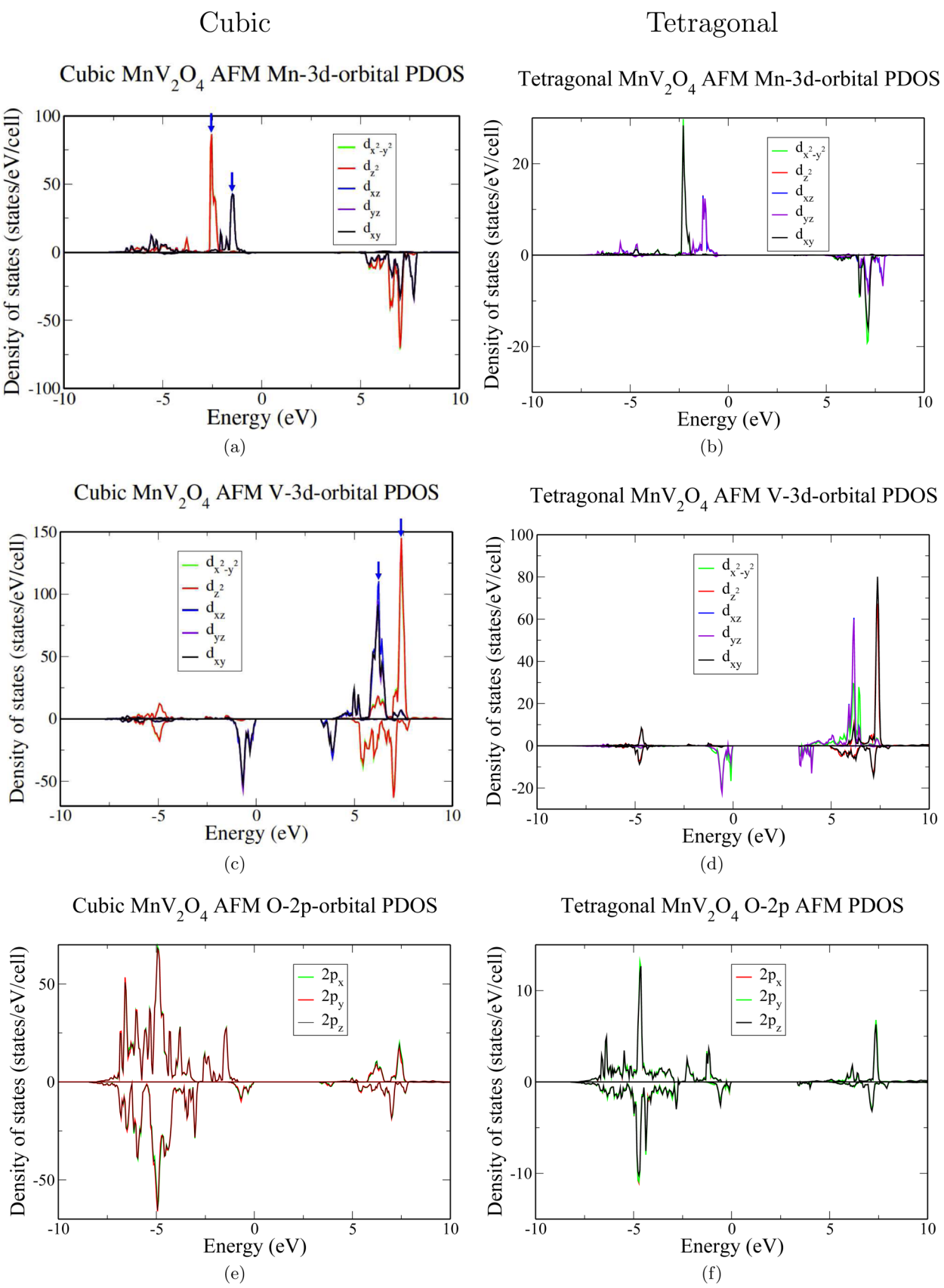

FIG. 2. (Color online) The PDOSs of the 3*d* orbitals on Mn, the 3*d* orbitals on V, and the 2*p* orbitals on O of the (left) cubic and (right) tetragonal MnV_2O_4 are shown. The PDOS onto $d_{x^2-y^2}$ is in green, d_{z^2} in red, d_{xz} in blue, d_{yz} in purple, and d_{xy} in black. For 2*p* orbitals, the PDOS onto $2p_x$ is in green, $2p_y$ in red, and $2p_z$ in black. In (g) and (h), the total PDOS onto Mn *d* orbitals is in red, V *d* orbitals in green, and O 2*p* orbitals in black.

The on-site Coulomb interaction U can be approximated by observing the gap between lower Hubbard d bands and the upper ones (∼5 eV for the Mn site and ∼7 eV for V), which is much larger than the crystal-field splitting computed here. This large Coulomb repulsion may facilitate the formation of the high-spin state for Mn^{2+} and V^{3+} ions, as suggested by previous experiments [11].

B. Exchange interactions

The magnetic structure could be much more complicated owing to the exchange interaction between the nearest-neighboring Mn (V) atoms [13] and the spin-orbit coupling (SOC), which will cause the noncollinear magnetic ordering. However, this topic is beyond the scope of this paper, which is focused on the electronic structure and the collinear magnetic ground state. The Mulliken spin densities on the Mn and V sites for cubic (tetragonal) MnV_2O_4 are $4.8\mu_B$ ($4.7\mu_B$) and $-2.0\mu_B$ ($-1.9\mu_B$), respectively. They are close to the expected values, i.e., $5\mu_B$ for Mn and $-2\mu_B$ for V (antialigned). For the cubic (tetragonal) structure, the computed total energies for a conventional cell with the spins on Mn and V aligned (ferromagnetic) are higher than those for antialigned spins (AFM) by 937 meV (754 meV). This in turn gives an approximate exchange interaction of ∼38 meV (divided by the factor $4 \times S_{Mn} \times S_V = 20$, where 4 is the number of Mn-V pairs in the unit cell for the tetragonal structure). Similarly, we can estimate the exchange interaction for the cubic structure, which is ∼23 meV. On the other hand, the exchange interaction between the Mn and V spins can also be estimated by using the superexchange formalism, where $4t$ can be quantified in the PDOS, which is ∼0.5 eV for Mn and ∼1 eV for V. By using these hopping integrals, the exchange interaction can be estimated as $\frac{t_{Mn}t_V}{\overline{U}}$ ($\overline{U} = \frac{U_{Mn}+U_V}{2}$), which is ∼4 meV. This is on the same order as the energy scale of the Néel temperature (50 K) previously mentioned (here an average value is taken for on-site Coulomb interaction). A detailed discussion of the exchange interaction, taking into account all the d orbitals on both Mn and V, would be great but is beyond the scope of this paper.

C. Orbital ordering

The OO in cubic and tetragonal MnV_2O_4 can be illustrated by the spin densities on V (see Fig. 3): the difference between the charge densities of spin-up and spin-down orbitals (essentially the charge densities of the spin-carry orbitals). In the tetragonal structure, the relative orientation rotation of neighboring orbitals is illustrated by the red arrows in Fig. 3(b); this is consistent with the previous calculations presented in Ref. [12], in which an antiferro-orbital ordering (AFOO) was predicted. The orbital orientations for the nearest-neighboring (NN) orbitals are perpendicular to each other (defined as AFOO). In sharp contrast, for the cubic structure the NN orbitals [labeled by X and Y in Fig. 3(a)] are organized in an exotic way, in which the orbitals on one of the four

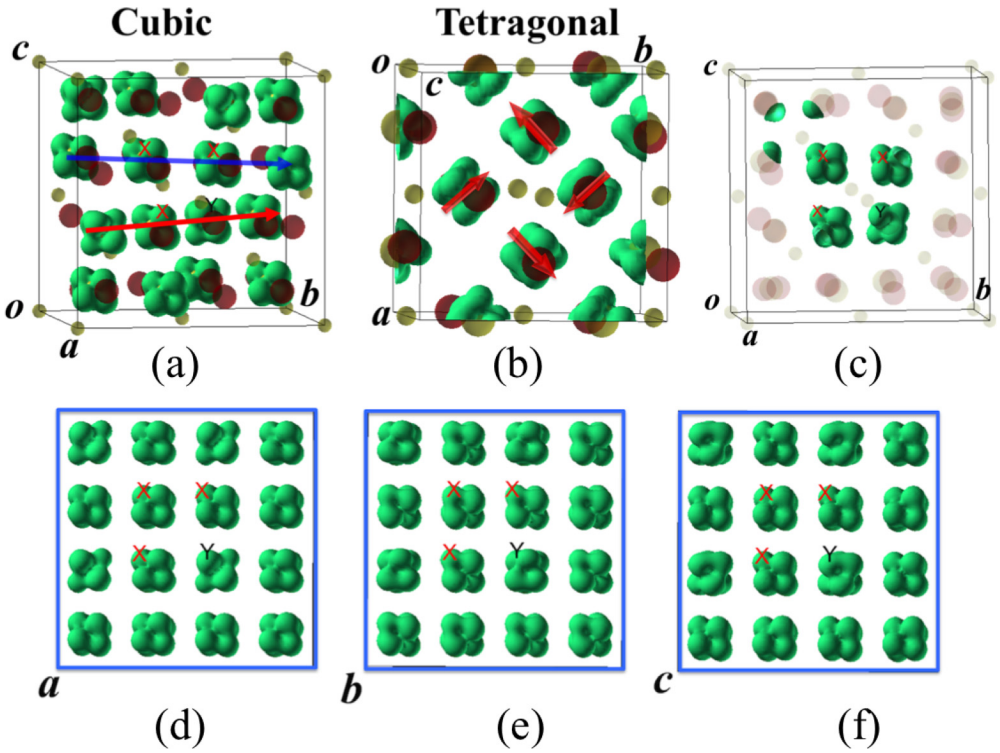

FIG. 3. (Color online) The spin densities on V of the AFM state in the conventional unit cell of the (a) cubic and (b) tetragonal structures of MnV_2O_4 are shown. In the tetragonal structure an antiferro-orbital ordering is found. In contrast, in the cubic structure, the rotation of the orbital orientation illustrates an exotic OO, in which a ferro-orbital ordering is along [110], while antiferro-orbital ordering is along [$\bar{1}$10]. This exotic OO is further confirmed by the calculation from the B3LYP functional; the resulting spin densities are shown in (c). The B3LYP spin-density calculation is performed in a unit cell but is shown in a conventional cell. The views from [100] ($\vec{a}$), [010] ($\vec{b}$), [001] ($\vec{c}$) lattice directions are shown in (d), (e), and (f), respectively. The isovalue is chosen as $0.04e/\text{Å}^3$.

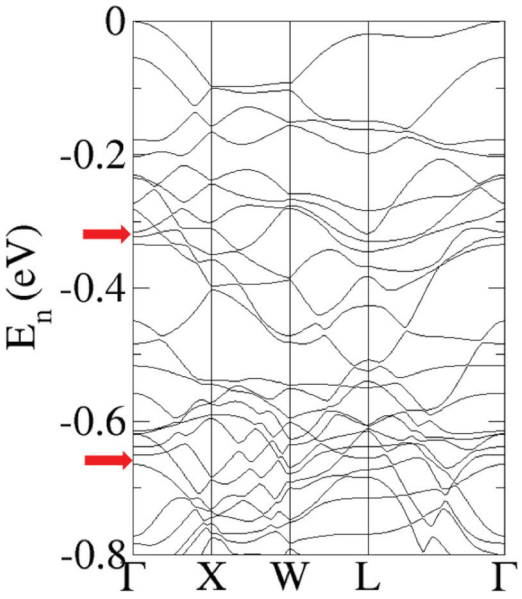

FIG. 4. (Color online) The spin-down band structure (from −0.8 to 0 eV) of the AFM configuration in the cubic MnV_2O_4 is shown. Note that the two red arrows refer to VB-8 and VB-9 and VB-19 and VB-20, respectively.

symmetry-inequivalent V atoms in the unit cell have a different orbital orientation (labeled by Y), perpendicular to the others (labeled by X). The orbital orientations corresponding to Fig. 3(a) are further illustrated in Figs. 3(d), 3(e), and 3(f), which are the views of the spin densities from the lattice directions [100] ($\vec{a}$), [010] ($\vec{b}$), and [001] ($\vec{c}$), respectively. This leads to an exotic OO: a ferro-OO (FOO) along [110] (blue arrow in Fig. 3) and an AFOO along [$\bar{1}$10] (red arrow in Fig. 3). This OO can probably be attributed to (i) the crystal-field environment formed by neighboring oxygen atoms and (ii) the Coulomb interaction between d orbitals. This interesting OO has been further confirmed by calculations with a different type of exchange-correlation functional, Becke three-parameter Lee-Yang-Parr (B3LYP) [34], which relies on the empirical parameters for mixing exact exchange and the GGA exchange functional. The spin densities on V predicted using the B3LYP functional are shown in Fig. 3(c), in which FOO is along [110] and AFOO is along [$\bar{1}$10] (all the atoms are made partially transparent in order to illustrate OO).

To see the orbitals involved in the OO of cubic MnV_2O_4 more clearly, the atomic orbital compositions of the bands (see Fig. 4) at the Γ point that contribute most to the two peaks at −0.26 and −0.64 eV in the V spin-down PDOS [see Fig. 2(c)] have been investigated. The bands VB − 8 and VB − 9 contribute the most to the peak at −0.26 eV, whereas VB − 19 and VB − 20 contribute most to the one at −0.64 eV. Although the atomic coefficients for d orbitals are slightly different among V atoms, approximately, the most dominant linear combinations of d orbitals for each V atom contained in these bands read

$$\phi_{\text{VB-8}} = 0.2|d_{xz}\rangle + 0.1|d_{yz}\rangle + 0.2|d_{xy}\rangle, \quad (1)$$

$$\phi_{\text{VB-9}} = -0.1|d_{xz}\rangle + 0.2|d_{yz}\rangle - 0.2|d_{xy}\rangle, \quad (2)$$

$$\phi_{\text{VB-19}} = 0.2|d_{xz}\rangle - 0.1|d_{yz}\rangle - 0.2|d_{xy}\rangle, \quad (3)$$

$$\phi_{\text{VB-20}} = 0.2|d_{xz}\rangle + 0.2|d_{yz}\rangle + 0.1|d_{xy}\rangle. \quad (4)$$

The corresponding spherical harmonic functions have been plotted in Fig. 5 to see the contributions of d orbitals. From the perspectives of linear combination of atomic orbitals (LCAO), the strong variations of the orbital orientation illustrated in Figs. 3 and 5 result from the minimization of the total energy respective to atomic orbital coefficients. On the other hand, the process of energy minimization can be seen as the orbital reorientation driven by Coulomb and crystal-field interactions.

There are two concepts that are closely related to this exotic orbital ordering, including orbital-glass and -ice states. The orbital-glass state is formed by the randomly orientated orbitals, which result from Jahn-Teller distortion and orbital frustrations in a manner similar to spin frustrations [16,17]. In light of the fact that orbital-glass states have been observed in spinel compounds $FeCr_2S_4$ and $LuFe_2O_4$ [16,17] (which have a chemical formula similar to that of a spinel but with a different structure), this is not completely unexpected in cubic MnV_2O_4. Therefore, these calculations could suggest that at $T = 53$ K, there is not only a structural transition but also an orbital-ordering transition from the exotic OO illustrated

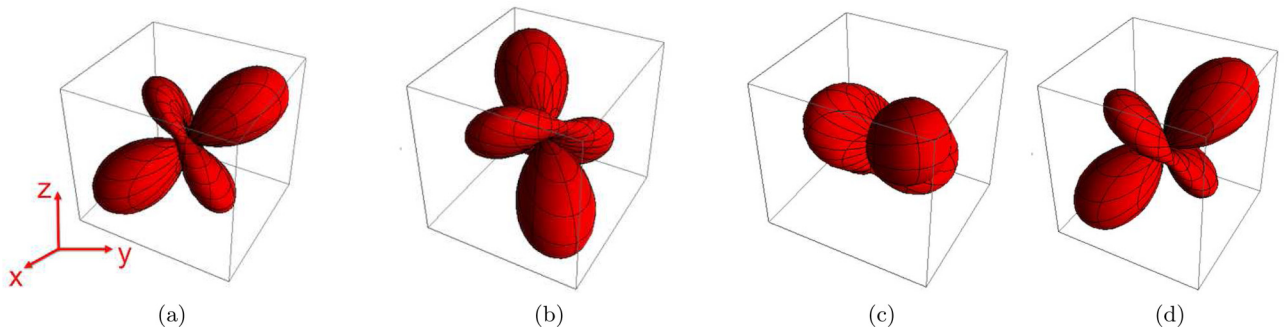

FIG. 5. (Color online) The linear combination of harmonic spherical functions is shown. $2Y_{xz} + Y_{yz} + 2Y_{xy}$ [corresponding to Eq. (1)] are shown in (a), $-Y_{xz} + 2Y_{yz} - 2Y_{xy}$ [corresponding to Eq. (2)] are shown in (b), $2Y_{xz} - Y_{yz} - 2Y_{xy}$ [corresponding to Eq. (3)] are shown in (c), and $2Y_{xz} + 2Y_{yz} + Y_{xy}$ [corresponding to Eq. (4)] are shown in (d). Notice that the linear combination illustrated in (c) changes the orientation of orbitals significantly away from their original ones, which is closely related to the exotic OO shown in Fig. 3(a).

in Fig. 3 to antiferro-orbital ordering [12] as temperature decreases. In addition, Chern and Wu have presented an ice model consisting of triplet orbital variables (such as p orbitals), which is, however, closely related to orbital-driven many-body phenomena in optical lattice [18]. The analog of a spin-interacting Hamiltonian, an orbital-exchange model describing Coulomb interactions, has been used therein. The exotic ordering presented here is closely related to the newly proposed concept of orbital ice [18], which is similar to spin ice.

IV. CONCLUSION

The electronic structures of the cubic and tetragonal MnV_2O_4 structures have been computed using hybrid-exchange density-functional theory (PBE0 and B3LYP). The calculated PDOS of the tetragonal structure is in good agreement with previous theoretical results. The most important finding here is that the charge densities of spin-carrying orbitals suggest the possible existence of an exotic orbital ordering: FOO along [110] and AFOO along [$\bar{1}$10] in cubic MnV_2O_4. The theoretical prediction presented here could be validated in a future experiment. For example, the different OOs along those two lattice orientations could lead to different electron transport properties. More advanced theoretical methods such as dynamical mean-field theory [35] are also needed to further understand the electronic structure of MnV_2O_4. In the ground state the spins on Mn and V are predicted to be antialigned, suggesting a ferrimagnetic state for both structures, which is in good agreement with previous theoretical and experimental results. The lower and upper Hubbard bands of Mn and V d electrons have been shown clearly below and above the band gap. The on-site Coulomb interaction can be estimated by using the gap between the lower and upper Hubbard bands, which is $\sim$7 eV for V and $\sim$5 eV for Mn. The transfer integral responsible for the delocalization is on the order of 1 eV, which should be attributed to a combination of first-order direct hopping between Mn and V and the second-order effect via O atoms.

ACKNOWLEDGMENTS

I would like to acknowledge the stimulating discussions with Dr. L. Bernasconi, Dr. B. Chen, and Dr. J. Laverock. I also thank B. Searle for technical support and Rutherford Appleton Laboratory for computational resources. I wish to acknowledge the support of the UK research councils grant (No. EP/J018473/1).

[1] J. G. Bednorz and K. A. Mller, Z. Phys. B **64**, 189 (1986).
[2] M. K. Wu, J. R. Ashburn, C. J. Torng, P. H. Hor, R. L. Meng, L. Gao, Z. J. Huang, Y. Q. Wang, and C. W. Chu, Phys. Rev. Lett. **58**, 908 (1987).
[3] E. J. W. Verwey, Nature (London) **144**, 327 (1939).
[4] I. D. Khomskii and M. V. Mostovoy, J. Phys. A **36**, 9197 (2003).
[5] A. I. Liechtenstein, V. I. Anisimov, and J. Zaanen, Phys. Rev. B **52**, R5467(R) (1995).
[6] J. B. Goodenough, Phys. Rev. **100**, 564 (1955).
[7] K. I. Kugel and I. D. Khomskii, Sov. Phys. Solid State **17**, 285 (1975).
[8] E. D. Mun, G.-W. Chern, V. Pardo, F. Rivadulla, R. Sinclair, H. D. Zhou, V. S. Zapf, and C. D. Batista, Phys. Rev. Lett. **112**, 017207 (2014).
[9] Y. Huang, Z. Yang, and Y. Zhang, J. Phys. Condens. Matter **24**, 056003 (2012).
[10] S. Kawaguchi, H. Ishibashi, S. Nishihara, M. Miyagawa, K. Inoue, S. Mori, and Y. Kubota, J. Phys. Condens. Matter **25**, 416005 (2013).
[11] K. Adachi, T. Suzuki, K. Kato, K. Osaka, M. Takata, and T. Katsufuji, Phys. Rev. Lett. **95**, 197202 (2005).
[12] S. Sarkar, T. Maitra, R. Valentí, and T. Saha-Dasgupta, Phys. Rev. Lett. **102**, 216405 (2009).
[13] Y. Nii, N. Abe, and T. H. Arima, Phys. Rev. B **87**, 085111 (2013).
[14] D. Felbacq and M. Antezza, SPIE Newsroom (2012).
[15] P. W. Anderson, Phys. Rev **102**, 1008 (1956).
[16] R. Fichtl, V. Tsurkan, P. Lunkenheimer, J. Hemberger, V. Fritsch, H.-A. Krug von Nidda, E.-W. Scheidt, and A. Loidl, Phys. Rev. Lett. **94**, 027601 (2005).
[17] A. M. Mulders, S. M. Lawrence, U. Staub, M. Garcia-Fernandez, V. Scagnoli, C. Mazzoli, E. Pomjakushina, K. Conder, and Y. Wang, Phys. Rev. Lett. **103**, 077602 (2009).
[18] G.-W. Chern and C. Wu, Phys. Rev. E **84**, 061127 (2011).
[19] B. A. Bernevig, T. L. Hughes, and S.-C. Zhang, Phys. Rev. Lett. **95**, 066601 (2005).
[20] V. O. Garlea, R. Jin, D. Mandrus, B. Roessli, Q. Huang, M. Miller, A. J. Schultz, and S. E. Nagler, Phys. Rev. Lett. **100**, 066404 (2008).
[21] T. Suzuki, M. Katsumura, K. Taniguchi, T. Arima, and T. Katsufuji, Phys. Rev. Lett. **98**, 127203 (2007).
[22] G.-W. Chern, N. Perkins, and Z. Hao, Phys. Rev. B **81**, 125127 (2010).
[23] B. Chen, J. Laverock, D. Newby, Jr., T.-Y. Su, K. E. Smith, W. Wu, L. H. Doerrer, N. F. Quackenbush, S. Sallis, L. F. J. Piper, D. A. Fischer, and J. C. Woicik, J. Phys. Chem. C **118**, 1081 (2014).
[24] M. Serri, W. Wu, L. Fleet, N. M. Harrison, C. W. Kay, A. J. Fisher, C. Hirjibehedin, G. Aeppli, and S. Heutz, Nat. Commun. **5**, 3079 (2014).
[25] C. Adamo and V. Barone, J. Chem. Phys. **110**, 6158 (1999).
[26] R. Dovesi, V. R. Saunders, C. Roetti, R. Orlando, C. M. Zicovich-Wilson, F. Pascale, B. Civalleri, K. Doll, N. M. Harrison, I. J. Bush, P. D'Arco, and M. Llunell, CRYSTAL09 (University of Turin, Turin, Italy, 2009).
[27] M. F. Peintinger, D. V. Oliveira, and T. Bredow, J. Comput. Chem. **34**, 451 (2012).
[28] W. C. Mackrodt, N. M. Harrison, V. R. Saunders, N. L. Allan, M. D. Towler, E. Apra', and R. Dovesi, Philos. Mag. A **68**, 653 (1993).
[29] M. D. Towler, N. L. Allan, N. M. Harrison, V. R. Saunders, W. C. Mackrodt, and E. Apra', Phys. Rev. B **50**, 5041 (1994).

[30] H. J. Monkhorst and J. D. Pack, Phys. Rev. B **13**, 5188 (1976).
[31] L. Noodleman, J. Chem. Phys. **74**, 5737 (1981).
[32] A. Kismarahardja, J. S. Brooks, H. D. Zhou, E. S. Choi, K. Matsubayashi, and Y. Uwatoko, Phys. Rev. B **87**, 054432 (2013).
[33] B. Chen, J. Laverock, W. Wu, J. Kuyyalil, D. Newby, Jr., K. E. Smith, R. M. Qiao, W. Yang, L. D. Tung, R. P. Singh, and G. Balakrishnan (unpublished).
[34] A. D. Becke, J. Chem. Phys. **98**, 5648 (1993).
[35] G. Kotliar, S. Y. Savrasov, K. Haule, V. S. Oudovenko, O. Parcollet, and C. A. Marianetti, Rev. Mod. Phys. **78**, 865 (2006).